Scripta Materialia 127 (2017) 58–62

Contents lists available at ScienceDirect

Scripta Materialia

journal homepage: www.elsevier.com/locate/scriptamat

Regular Article

Solidification path of single-crystal nickel-base superalloys with minor carbon additions under laser rapid directional solidification conditions

Yao-Jian Liang, Jia Li *, An Li, Xiao-Tong Pang, Hua-Ming Wang

National Engineering Laboratory of Additive Manufacturing for Large Metallic Components and Engineering Research Center of Ministry of Education on Laser Direct Manufacturing for Large Metallic Components, School of Materials Science and Engineering, Beihang University, 37 Xueyuan Road, Beijing 100191, People's Republic of China

ARTICLE INFO

Article history:
Received 25 June 2016
Received in revised form 31 August 2016
Accepted 31 August 2016
Available online xxxx

Keywords:
Laser treatment
Superalloy
Rapid directional solidification
Solidification microstructure
Phase transformations

ABSTRACT

The solidification path of single-crystal nickel-base superalloys containing minor carbon was investigated under various laser rapid directional solidification (LRDS) conditions. By controlling the solidification rate, LRDS processing can provide the evidence whether some diffusion-controlled phase transformations occur because such transformations will be suppressed under high cooling rates. Results show that the solidification path and final solidification microstructure depend upon the cooling rate; the microstructure without γ-γ′ eutectic can be obtained as long as the cooling rate is high enough. A peritectic transformation in carbon-containing single-crystal superalloys was first experimentally verified by controlling the cooling rate during LRDS processing.

Single-crystal (SX) nickel-base superalloys are widely used in turbine engines due to their excellent mechanical properties at elevated temperatures. Although carbon, a grain boundary strengthener, was fully eliminated from early SX superalloys, minor additions of carbon (≤0.05 wt%) have been reintroduced to a number of commercial SX alloys because of the frequent existence of low-angle grain boundaries [1,2]. Moreover, recent research by Tin and Pollock et al. [3–6] has confirmed that under conventional DS conditions, minor carbon additions to high-refractory SX superalloys are beneficial to lower the tendency of grain-defect formation and refractory element segregation. Hence, it is desirable to understand the solidification behavior of these SX alloys containing minor carbon because it is critical for the control of their final solidification microstructure and mechanical properties.

Recently, laser processing, *e.g.*, laser additive manufacturing (LAM), has exhibited its potential for precise repair and rapid forming of SX components [7–16] with high solidification cooling rates [17–19]. It is well known that rapid solidification (RS) processing is an effective way to reduce microsegregation and refine microstructure. More importantly, by controlling solidification velocity, RS processing can provide the evidence whether some diffusion-controlled phase transformations occur because these transformations will be suppressed under high solidification rates [20]. It is therefore specifically appropriate to be used to investigate solidification phase transformations. With this in mind, of particular interest is the effect of minor carbon additions on the solidification sequence of SX superalloys under laser rapid directional solidification (LRDS) conditions. Unfortunately, although many researchers have focused on the morphology and growth mechanism of MC carbides [21,22] and on the solidification behaviors of early DS superalloys with relatively high carbon contents [23,24], the solidification path of the SX superalloys with minor carbon additions has not yet been reported under LRDS conditions. Consequently, the main objective of this study is to reveal the solidification sequence of the SX nickel-base superalloys with minor carbon additions under RS conditions. For this purpose, a SX superalloy containing minor carbon was treated under various LRDS conditions to understand its RS path.

To obtain various LRDS conditions, laser remelting experiments were conducted with different processing parameters (Table 1) by a 6 kW LAM system with an oxygen content < 50 ppm. The chemical composition of the SX Ni-base superalloy studied here is Ni–5.7Al–9.2Cr–5.3Co–2.7Ta–2.3Ti–8.9W–0.015C (in wt%). All SX substrates were machined from a conventional DS SX cast ingot with the [001] orientation normal to the remelted surfaces. For all experiments, the substrate surfaces were ground with 600-grit SiC paper, cleaned in methanol, and maintained at room temperature prior to laser remelting. In order to relate a set of given laser processing parameters to resulting solidification behavior, the temperature gradient was estimated by the laser temperature field, and the solidification velocity was related to the laser scanning velocity and melt-pool geometry, where the temperature field and melt-pool geometry were given by a laser-remelted heat-transfer equation reported elsewhere [11,15]. Subsequently, mean temperature gradient, G_M, and solidification velocity, V_M, were calculated over the total melt-pool depth along the symmetrical centerline of liquidus isotherm. Corresponding mean cooling rates in melt pools, R_C, listed in

* Corresponding author.
E-mail address: lijia@buaa.edu.cn (J. Li).

http://dx.doi.org/10.1016/j.scriptamat.2016.08.039
1359-6462/

Table 1
Laser processing parameters (laser power, P, scanning velocity, V_b, and beam diameter, D_b) and corresponding cooling rate, R_C.

No.	P (W)	V_b (mm/s)	D_b (mm)	R_C (K/s)
A	2000	5	4	1101.1
B	2000	45	2	17,606.4

Table 1, can be obtained by $R_C = dT/dt = G_M \cdot V_M$, where T is the temperature and t is the time [20]. The microstructures were characterized by a CamScan Apollo300 field emission scanning electron microscope (SEM) equipped with an Oxford INCA energy dispersive spectrometer (EDS). The thermal characteristics of the samples were investigated by a Netzsch STA-449F3 differential scanning calorimetry (DSC) instrument on heating.

Fig. 1a and b shows the solidification microstructures of the LRDS SX samples. Both the two processing conditions can produce good rapid directional solidification microstructures. The fine dendrites grow epitaxially from the SX substrates to the top of laser tracks along the [001]/〈100〉 crystallographic orientation. For investigating the solidification path of the RS carbon-containing SX alloys, Fig. 1c and d shows the cross-section dendritic morphologies of the two samples. As shown in Fig. 1c, with minor carbon additions, some white, branching precipitates occur in the interdendritic regions of epitaxial γ dendrites in sample A. The DSC profiles show that there is a reaction peak at ~1612 K just below the liquidus (~1635 K), which was identified as a γ-MC eutectic peak in earlier research [3–6] and verifies these phases formed after the growth of γ dendrites to be MC carbides. Similar to earlier research [21,22], the EDS analysis shows that these carbides are mainly Ti- and Ta-rich. In comparison, owing to a great increase in cooling rate, the primary dendrites are finer and the carbides distributed in the interdendritic regions of sample B become non-branching, small rods (or layers) (see Fig. 1d). Additionally, the porosity in sample B is visibly higher than that in sample A. This appears to be because as solidification velocity increases, residual liquid has no enough time to fill up the interdendritic regions. Even so, their solidification times are rather short compared with conventional DS process, which implies that there exist other reasons affecting the porosity and they will be discussed later. It is also noteworthy that no visible γ-γ′ eutectic is found in Fig. 1. However, the last stage solidification is generally considered to be completed by forming the γ-γ′ eutectic microstructure in earlier research on the solidification behaviors of welded superalloys with relatively high carbon contents by Ojo and Sidhu et al. [23,24]. Therefore, the understanding of the solidification path of the LRDS SX alloys with a low carbon content requires careful investigations into the interdendritic microstructures.

In order to assess the solidification sequence, the LRDS microstructures at interdendritic regions of samples A and B are shown in Fig. 2a and b, respectively. The branching morphology of the MC carbides can be seen more clearly in Fig. 2a. It is interesting that a small number of γ-γ′ eutectic islands are found, as shown in the middle-top of the figure. Compared with sample A, the branches of the MC carbides in sample B are not visible and no γ-γ′ eutectic is observed. To better understand the solidification sequence, Fig. 2c illustrates the back-scattered electron (BSE) image of the interdendritic region same as Fig. 2a. As can be seen, the γ-γ′ eutectic is very close to (or even locates at) interdendritic shrinkage defects, which implies that the initiation of these reactions indeed lags behind the precipitation of the MC carbides. In particular, a few MC carbides are observed to be wrapped in these γ-γ′ eutectic microstructures and this characteristic can be seen more clearly in a high-magnification view (Fig. 2d). However, such a microstructure is not found in the conventional DS SX substrate with a low cooling rate though the MC carbides also adjoin the γ-γ′ eutectic islands (see Fig. 2e).

According to above careful analyses of solidification microstructure, the solidification paths of the SX superalloy containing minor carbon under various LRDS conditions can be proposed by using a simplified pseudo-ternary composition triangle of γ, γ′, and MC similar to previous research [23,25] (Fig. 3a).

Step I. Solidification commences with the well-known phase transformation, $L \rightarrow \gamma_0$. As a result, the solidification microstructure of the LRDS SX exhibits mostly γ dendrites epitaxially growing from the SX

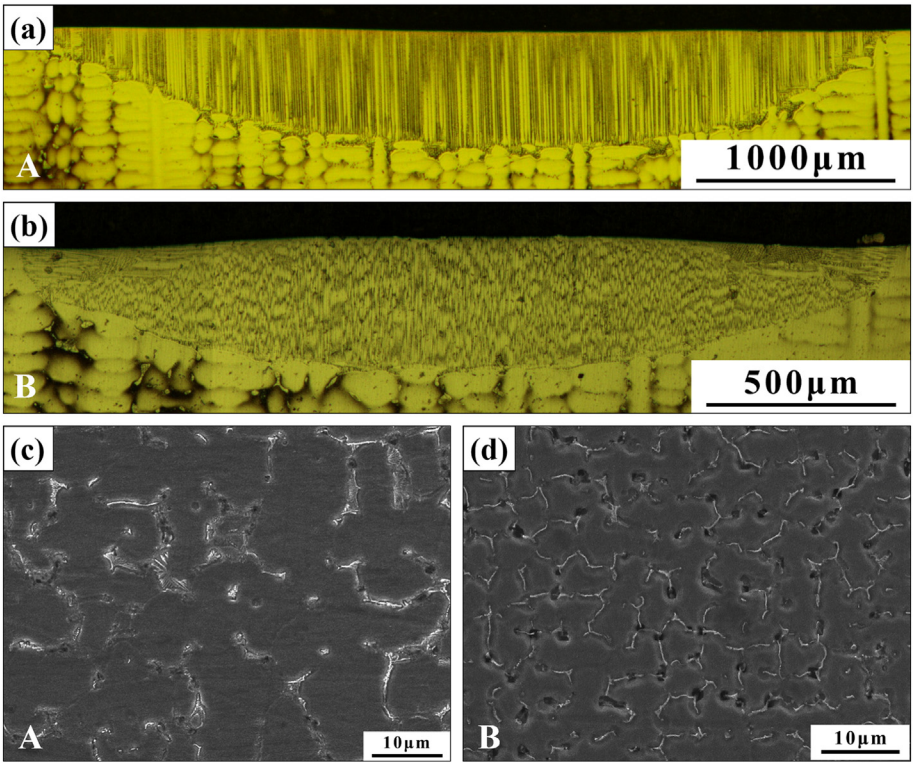

Fig. 1. OM images showing the solidification microstructures of the LRDS SX samples: (a) A and (b) B. SEM images of the cross-section dendritic morphologies of samples (c) A and (d) B.